Available online at www.sciencedirect.com
ScienceDirect
International Journal of Heat and Mass Transfer 51 (2008) 5497–5510
International Journal of HEAT and MASS TRANSFER
www.elsevier.com/locate/ijhmt

A mathematical model for skin burn injury induced by radiation heating

Weizhong Dai [a,*], Haojie Wang [a], Pedro M. Jordan [b], Ronald E. Mickens [c], Adrian Bejan [d]

[a] Mathematics and Statistics, Louisiana Tech University, Ruston, LA 71272, USA
[b] Code 7181, Naval Research Laboratory, Stennis Space Center, MS 39529-5004, USA
[c] Department of Physics, Clark Atlanta University, Atlanta, GA 30314, USA
[d] Department of Mechanical Engineering and Materials Science, Duke University, Durham, NC 27708-0300, USA

Received 4 May 2007; received in revised form 2 January 2008
Available online 4 March 2008

Abstract

We modify the Pennes model by taking into account the thermal relaxation time of biological tissue. Specifically, we employ the Maxwell–Cattaneo thermal flux law, in conjunction with the fourth power law, to model the effects of high thermal radiation on such skin. The skin is considered to be a 3D triple-layered structure with embedded dendritic countercurrent multi-level blood vessels, artery and vein, where the dimensions and blood flow of the multi-level blood vessels are determined based on the constructal theory of multi-scale tree-shaped heat exchangers. The method is illustrated by a numerical example.
© 2008 Elsevier Ltd. All rights reserved.

1. Introduction

High thermal radiation produced by intense fire is often encountered in daily life, e.g., wild fires and chemical fires. Understanding the effect of high thermal radiation on biological bodies, specifically, thermomechanical damage to tissue, requires the accurate description of bioheat transfer. It is known that heat transfer within the human body is a complicated process involving metabolic heat generation, heat conduction and blood perfusion in soft tissue, convection and perfusion of the arterial-venous blood through the capillary, and interaction with the environment. The modeling of heat-related phenomena such as bioheat transfer and heat-induced stress is of great importance for the development of biological and biomedical technologies, such as thermotherapy and the design of heating or cooling garments, as well as protecting human life in cases of accidental or natural disasters [1,2].

In the early 1990s, it was discovered that biological tissue, along with a number of other common materials, exhibited a relatively long thermal relaxation (or lag) time, often denoted by τ (see [3]). Physically, τ represents the time required to establish steady thermal conduction in a material volume element once a temperature gradient has been imposed across it. The implication of such large values of τ, which could range up to 100 s (see [4]), is that heat conduction in organic media is generally not described by Fourier's law, the classical expression for the thermal flux vector $\vec{q}$, but rather by the Maxwell–Cattaneo flux law [5–13], namely

$$\left(1+\tau\frac{\partial}{\partial t}\right)\vec{q}=-k\nabla T, \tag{1}$$

where k and T denote the thermal conductivity and tissue temperature, respectively. Eq. (1) predicts that heat conduction in such media occurs not by diffusion, but in a wave-like manner, a phenomena now known as "second sound" (again, see [5–13]).

The objective of this article is to develop a new mathematical model based on the Maxwell–Cattaneo flux law, along with numerical techniques, for predicting the "burning" (i.e., thermal damage) inflicted upon skin, as modeled

* Corresponding author. Tel.: +1 318 257 3301; fax: +1 318 257 2562.
E-mail address: dai@coes.latech.edu (W. Dai).

0017-9310/$ - see front matter © 2008 Elsevier Ltd. All rights reserved.
doi:10.1016/j.ijheatmasstransfer.2008.01.006

Nomenclature

B_i	Biot number
C_l, C_b^l	specific heat of tissue and blood in layer l
C_B	heat capacity of blood
F_m	area of cross-section in the mth level vessel
h	heat convection coefficient
k_l	heat conductivity of layer l
L_l	thickness of layer l
L_b^m	length of the blood vessel in level m along the flowing direction of blood
M_m	main flow of blood in the mth level vessel
N_x, N_y, N_l^z	numbers of grid points in the x, y, z directions, respectively
NX, NY	lengths of the skin structure in the x, y directions, respectively
NL_b^m, NW_b^m	length and width of the cross-section of the mth level vessel
P	vessel periphery
$\dot{P}$	blood flow rate
$(s_l)_{ijk}^n$	numerical solution of function S_l
T_b^m, T_l, T_w^m	temperatures in blood, tissue, and vessel wall, respectively
T_{in}, T_{out}	temperatures of blood at entrance and exit, respectively
T_a	ambient temperature
t	time
u_{ijk}^n	numerical solution of temperature of tissue
u_b^m	numerical solution of temperature of blood in the mth level vessel
v_m	velocity of blood flow in the mth level vessel
W_b^l	blood perfusion rate in layer l
x, y, z	Cartesian coordinates
α	heat transfer coefficient between blood and tissue
δ_x^2, δ_y^2, δ_z^2	second-order finite difference (FD) operators
Δx, Δy, Δz	mesh sizes of FD scheme for bioheat transfer model in the x, y, z directions
Δt	time increment used in calculating heat transfer
ε	emissivity
ω	relaxation factor
ρ_l	density of layer l
σ	Stefan–Boltzmann constant
τ	thermal lag time

as a 3D composite structure, exposed to high thermal radiation; and thus provide information on the effects of high thermal radiation on a biological tissue. Our method differs from existing methods [14–25] in that our mathematical model is based on Eq. (1), which takes into account the relatively large thermal relaxation time of biological tissue, in conjunction with the fourth power law. In addition, the skin model we consider is a 3D, triple-layered structure, wherein is embedded countercurrent multi-level dendritic blood vessels, arteries and veins.

And it should be noted that the dimensions and blood flow rates of the multi-level blood vessels have been determined based on the recently developed constructal theory of multi-scale tree-shaped heat exchangers [26–29].

2. Bioheat transfer model

Under Fourier's flux law, the governing equation that describes the thermal conduction in biological tissue is given by

$$\rho C\frac{\partial T}{\partial t} = -\nabla\cdot\vec{q} + W_b C_b(T_b - T) + Q, \tag{2}$$

$$\vec{q} = -k\nabla T, \tag{3}$$

where T is the tissue temperature; T_b is the blood temperature; ρ, C, and k denote the density, specific heat, and thermal conductivity of the tissue, respectively; Q is the volumetric heat; C_b is the specific heat of blood; and W_b is the blood perfusion rate. Substituting $\vec{q}$ in Eq. (3) into Eq. (2), one may obtain the well-known Pennes bioheat transfer equation [14]

$$\rho C\frac{\partial T}{\partial t} = -\nabla\cdot\vec{q} + W_b C_b(T_b - T) + Q. \tag{4}$$

If, in place of Fourier's law, we employ the Maxwell–Cattaneo flux law, Eq. (1), then a modified (i.e., hyperbolic) form of the Pennes equation is obtained as the PDE which governs bioheat transport. Furthermore, if the tissue medium is now taken to be skin, which we model here as a 3D, triple-layered (i.e., composite) structure, and where each layer is assumed to be a thermally conducting rigid body, then the bioheat transport equation that follows from the Maxwell–Cattaneo law can be written as follows [21,22]:

$$\rho_l C_l\left(\frac{\partial T_l}{\partial t} + \tau\frac{\partial^2 T_l}{\partial t^2}\right) + \tau W_b^l C_b^l\frac{\partial T_l}{\partial t} = k_l\left[\frac{\partial^2 T_l}{\partial x^2} + \frac{\partial^2 T_l}{\partial y^2} + \frac{\partial^2 T_l}{\partial z^2}\right] + W_b^l C_b^l(T_{out} - T_l) + Q_l, \quad l = 1,2,3, \tag{5}$$

where T_l is the temperature of the lth tissue layer; T_{out} is the blood temperature at exit or entrance of the third level vessel for the artery or vein; ρ_l, C_l, and k_l denote the density, specific heat, and thermal conductivity of the lth tissue layer, respectively; τ is the thermal relaxation time; C_b^l is the specific heat of blood; and W_b^l is the blood perfusion rate. And since we only consider radiation heating in the present study, all other internal heat sources Q_l are ignored. Here, we observe that when τ is zero, the above equation reduces to the Pennes equation [14].

According to the medical literature, the largest arteries of the skin are arranged in the form of a flat network in the subcutaneous tissue, immediately below the dermis.

The dermis is very sparingly supplied with capillaries and the capillary beds of skin lie immediately below the epidermis [30]. Fig. 1 shows a realistic skin structure configuration [31].

To simplify our computation, we consider the target region to be a rectangular structure embedded with two countercurrent multi-level blood vessels that cross through the subcutaneous layer from the bottom to the top, as shown in Fig. 2. Note that only large blood vessels can be seen in the subcutaneous, because the dermis layer consists of only capillaries and the contribution of these small vessels to the heat transfer can be ignored [32].

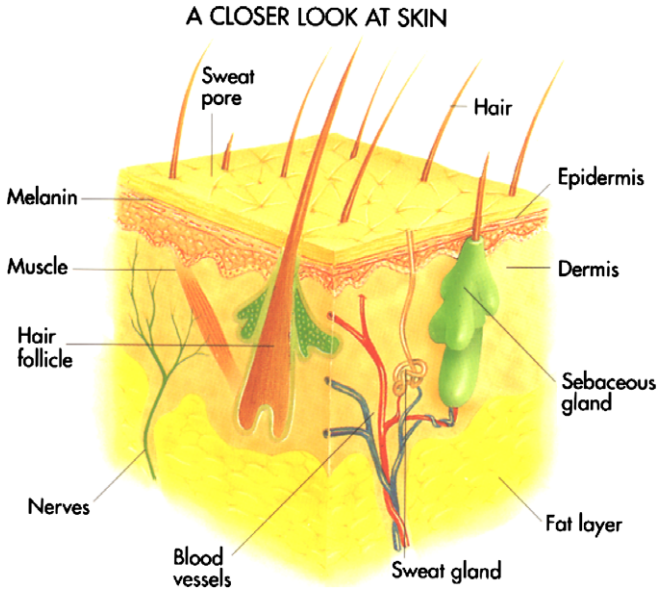

Fig. 1. A configuration of a skin structure.

In Fig. 2, the basic arterial model consists of the large central vessel (level 1) running lengthwise (in the z-direction) along the control volume. This vessel has a horizontal (in the x-direction) vessel (level 2) branching from it. The second vessel goes to third vessel (level 3) which runs again lengthwise (in the z-direction). The second vessel does not branch into two third vessels, and the diameters of these are also the same, which are similar to those in [33]. These vessels are modeled as slim cuboids for simplicity. The diameters of the arteries are assumed to be decreasing by a constant ratio γ between successive levels of branched vessels, which is given by [27]

$$\gamma = \frac{NL_b^2}{NL_b^1} = \frac{NW_b^2}{NW_b^1} = 2^{-\frac{1}{3}}, \tag{6}$$

Table 1
Parameters for a 3D skin structure [21,33,45,46]

Parameters	Values	Parameters	Values
α (W/°C cm^2)	0.2	k_2 (W/cm °C)	0.0052
C_1 (J/g °C)	3.6	k_3 (W/cm °C)	0.0021
C_2 (J/g °C)	3.4	$\dot{P}$ (1/s)	0.5×10^{-3}
C_3 (J/g °C)	3.06	v_1 (m/s)	0.08
C_b^1 (J/g °C)	0	W_b^1 (g/cm^3 s)	0
C_b^2 (J/g °C)	4.2	W_b^2 (g/cm^3 s)	0.0005
C_b^3 (J/g °C)	4.2	W_b^3 (g/cm^3 s)	0.0005
C_B (J/cm^3 · °C)	4.134	ρ_1 (g/cm^3)	1.2
h (W/cm^2)	0.001	ρ_2 (g/cm^3)	1.2
k_1 (W/cm °C)	0.0026	ρ_3 (g/cm^3)	1

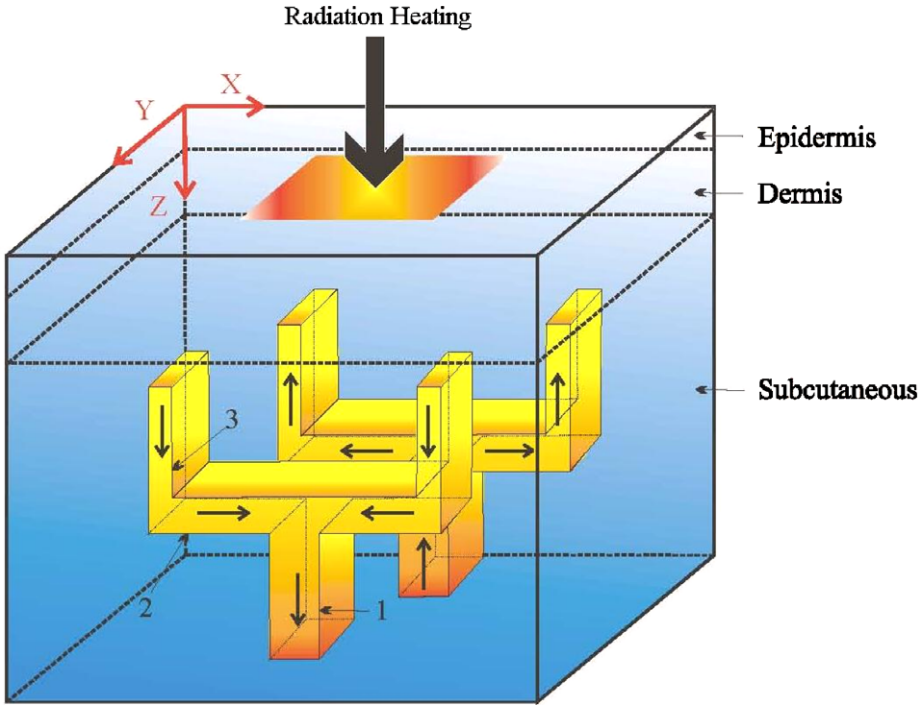

Fig. 2. A three-dimensional triple-layered skin structure embedded with countercurrent vasculature.

Table 2
Parameters used in computation

Parameters	Values	Parameters	Values
$B_i = \alpha/k_3$	95.23	T_a (°C)	200
L_1 (cm)	0.008	T_{in} (°C)	37
L_2 (cm)	0.2	ω	1
L_3 (cm)	1.0	Δx (cm)	0.02, 0.01
L_b^1 (cm)	0.4	Δy (cm)	0.02,0.01
L_b^2 (cm)	0.28	Δz (cm)	0.002
L_b^3 (cm)	0.2	Δt (s)	0.1
NX, NY (cm)	0.5	ε	0.9
NL_b^1, NW_b^1 (cm)	0.1	σ (W/m^2 K^4)	5.669×10^{-8}
NL_b^2, NW_b^2 (cm)	0.08	τ (s)	20
NL_b^3, NW_b^3 (cm)	0.08		
T_0 (°C)	34		

Table 3
Parameters used in Eq. (19) based on Takata's model [39]

Temperature range (°C)	$T \leqslant 50$	$T > 50$
Activation energy ΔE (J/K mol)	4.18×10^8	6.69×10^8
Scaling factor ζ (1/s)	4.322×10^{64}	6.69×10^{104}

where NL_b^m and NW_b^m are the length and width of the cross-section of a blood vessel in level m, respectively. The length of blood vessel is assumed to be double after two consecutive construction steps, which can be expressed in the length-doubling rule [28] as follows:

$$L_b^m = 2^{\frac{1}{2}} L_b^{m+1}, \quad m = 1, 2, \tag{7}$$

where L_b^m is the length of the blood vessel in level m. The mass flow of blood in the mth level vessel, $M_m = v_m F_m$, is assumed to satisfy [28],

$$M_1 = 2M_2, \quad M_2 = M_3, \tag{8}$$

where v_m is the blood flow velocity and F_m ($=NL_b^m \times NW_b^m$) is the area of the cross-section in the mth level vessel.

Furthermore, the blood temperature in the cross-section of a vessel is assumed to be uniform. We further assume that a steady-state energy balance in the blood vessel can be reached because the length of the considered blood vessel is relatively short and the blood velocity is relatively high. However, one may use a transient heat transfer equation for a more accurate solution. Hence, the convective

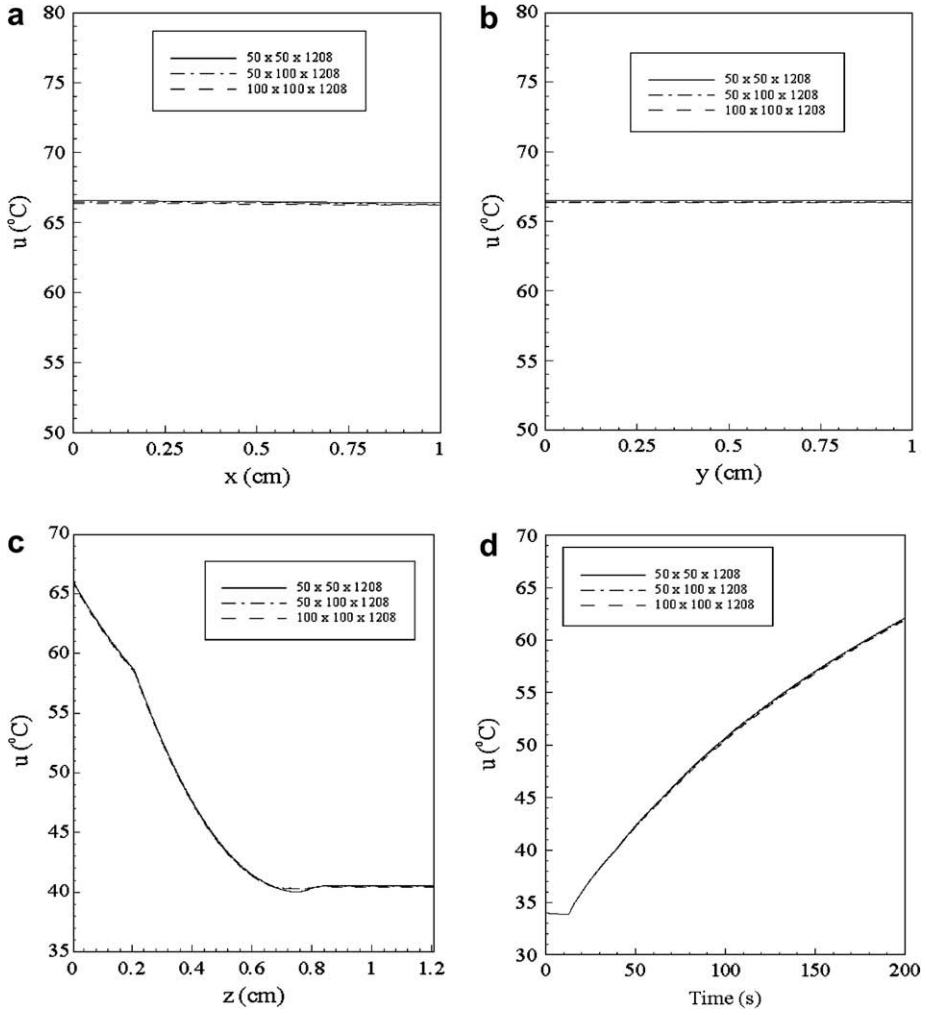

Fig. 3. Profiles of temperature at $t = 200$ s along lines: (a) at $y = 0.5$ cm, (b) at $x = 0.5$ cm, on the skin surface, and (c) along the depth (the z-direction) at the center of the skin surface, as well as (d) at the point with $x = 0.5$ cm, $y = 0.5$ cm, and $z = 0.1$ cm over time.

energy balance equations, which are used to calculate the main artery (levels 1 and 2) blood temperatures, can be expressed as [34,35]

$$C_B M_1 \frac{d(T_b^1)}{dz} - \alpha P_1 (T_w^1 - T_b^1) = 0, \tag{9}$$

and

$$C_B M_2 \frac{d(T_b^2)}{dx} - \alpha P_2 (T_w^2 - T_b^2) = 0, \tag{10}$$

where C_B is the heat capacity of blood, and α is the heat transfer coefficient between blood and tissue, and P_m is the vessel perimeter. Further, T_w^m and T_b^m are the wall temperature and the blood temperature in the mth level vessel. For the smallest, terminal arterial vessels (level 3), a decreased blood flow rate ($\dot{P}$) is included in the energy balance equation [34,35]

$$C_B M_3 \frac{d(T_b^3)}{dz} - \alpha P_3 (T_w^3 - T_b^3) - \dot{P} C_B F T_b^3 = 0. \tag{11}$$

For simplicity, the venous model is taken to be similar to the arterial model, except that the blood flow direction in the vein is opposite of that in the artery; i.e., countercurrent flow occurs in these two kinds of vessels (see Fig. 2). Also, the diameter ratio, length ratio, and mass flow ratio of the blood between the successive levels of the branched veins take the same form as described in Eqs. (6)–(8) for the arteries. Moreover, the convective energy balance equations (9)–(11) used to calculate the blood temperature in the artery domain is applied to the vein domain at the corresponding levels.

On the surface of the skin, we assume that heat exchange with the surroundings, which may include heat loss from convection and radiation [36], is described as follows:

$$-k_1 \frac{\partial T_1}{\partial z} = h(T_a - T_1) + \varepsilon\sigma(T_a^4 - T_1^4), \quad z = 0, \tag{12}$$

where h is the convective heat transfer coefficient, T_a is the ambient temperature, σ is the Stefan–Boltzmann constant, and ε is the emissivity. Because we consider radiation heating, the temperature T_a is much higher than T_1. And for simplicity, we assume that the heat flux approaches zero as the tissue depth increases, which is realistic for a biological body [21]. The other boundary conditions in the tissue are assumed to be

$$\frac{\partial T_1}{\partial \vec{n}} = 0, \tag{13}$$

where $\vec{n}$ is the unit outward normal vector on the boundary. At the entrance to the first level vessel, we have

$$T_b^1 = T_{in}, \tag{14}$$

where T_{in} is the blood temperature at the entrance of the artery. At the exit of the artery, we assume that the blood temperature is equal to the surrounding tissue temperature

$$T_b^3 = T_{out}. \tag{15}$$

Because the blood flow in the vein is oriented against the arterial flow, the entrance of the blood to the vein is located at the third level, and the blood temperature is equal to the surrounding tissue temperature.

The continuity of heat transfer between the lateral blood vessel and the tissue requires [37]

$$\frac{\partial T_b^m}{\partial \vec{n}} = B_i (T_w^m - T_b^m), \quad m = 1, 2, 3. \tag{16}$$

The interfacial continuity conditions between layers are given by

$$T_1 = T_2, \quad k_1 \frac{\partial T_1}{\partial z} = k_2 \frac{\partial T_2}{\partial z}, \quad z = L_1, \tag{17a}$$

$$T_2 = T_3, \quad k_2 \frac{\partial T_2}{\partial z} = k_3 \frac{\partial T_3}{\partial z}, \quad z = L_1 + L_2. \tag{17b}$$

The initial conditions are

$$T_l = T_0, \quad t = 0, \quad l = 1, 2, 3. \tag{18}$$

A quantitative description of thermal damage to skin, as suggested by Henriques and Mortiz [38], can be written as

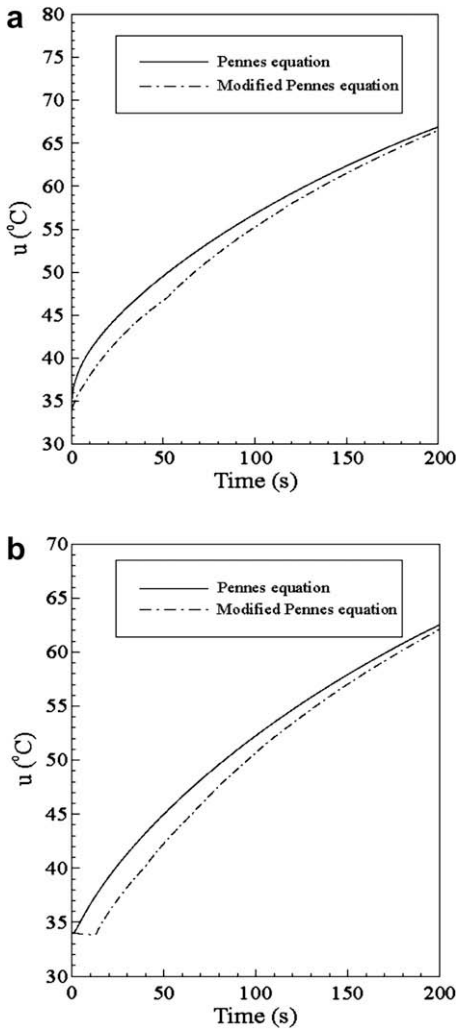

Fig. 4. Comparison of the solutions obtained by Pennes equation and the modified Pennes equation at locations: (a) $x = 0.5$ cm, $y = 0.5$ cm and $z = 0$ cm and (b) $x = 0.5$ cm, $y = 0.5$ cm and $z = 0.1$ cm.

$$\frac{\partial \Omega}{\partial t} = \zeta \exp\left(-\frac{\Delta E}{RT_l}\right), \tag{19}$$

where ζ is the frequency factor, ΔE is the activation energy controlling the development of tissue injury, and $R = 8.314472\ \mathrm{J\ K^{-1}\ mol^{-1}}$ is the gas constant. The temperature T_l is determined using Eq. (5). Here, we note that $\Omega = 0.53, 1.0, 10^4$ correspond to first, second, and third degree burn injuries, respectively [39].

3. Numerical method

We denote $(u_l)^n_{ijk}$ and u_b the numerical approximations of $(T_l)(i\Delta x, j\Delta y, k\Delta z, n\Delta t)$ and T_b, where Δx, Δy, Δz, and Δt are the spatial and temporal mesh sizes, and i, j, k are integers with $0 \leqslant i \leqslant N_x$, $0 \leqslant j \leqslant N_y$, $0 \leqslant k \leqslant N^z_l$, so that $N_x\Delta x = NX$, $N_y\Delta y = NY$, and $N^z_l\Delta z = L_l$, $l = 1, 2, 3$. In this mesh, we assume that $(u_3)^n_{ijk} = (u^m_b)_{ijk}$ when the grid point (i,j,k) is in the mth level blood vessel. Because Eqs. (9)–(11) are first-order ordinary differential equations once T^m_w is determined, they can be solved by using the fourth-order Runge–Kutta method [40]. To develop an unconditionally stable finite difference scheme for Eq. (5), we first follow the approach in [41,42] and introduce

$$S_l = \left(1 + \tau \frac{W^l_b C^l_b}{\rho_l C_l}\right) T_l + \tau \frac{\partial T_l}{\partial t}. \tag{20}$$

As such, Eq. (5) becomes

$$\rho_l C_l \frac{\partial S_l}{\partial t} = k_l \left[\frac{\partial^2 T_l}{\partial x^2} + \frac{\partial^2 T_l}{\partial y^2} + \frac{\partial^2 T_l}{\partial z^2}\right] + W^l_b C^l_b (T_{out} - T_l). \tag{21}$$

Discretizing Eqs. (20) and (21) gives

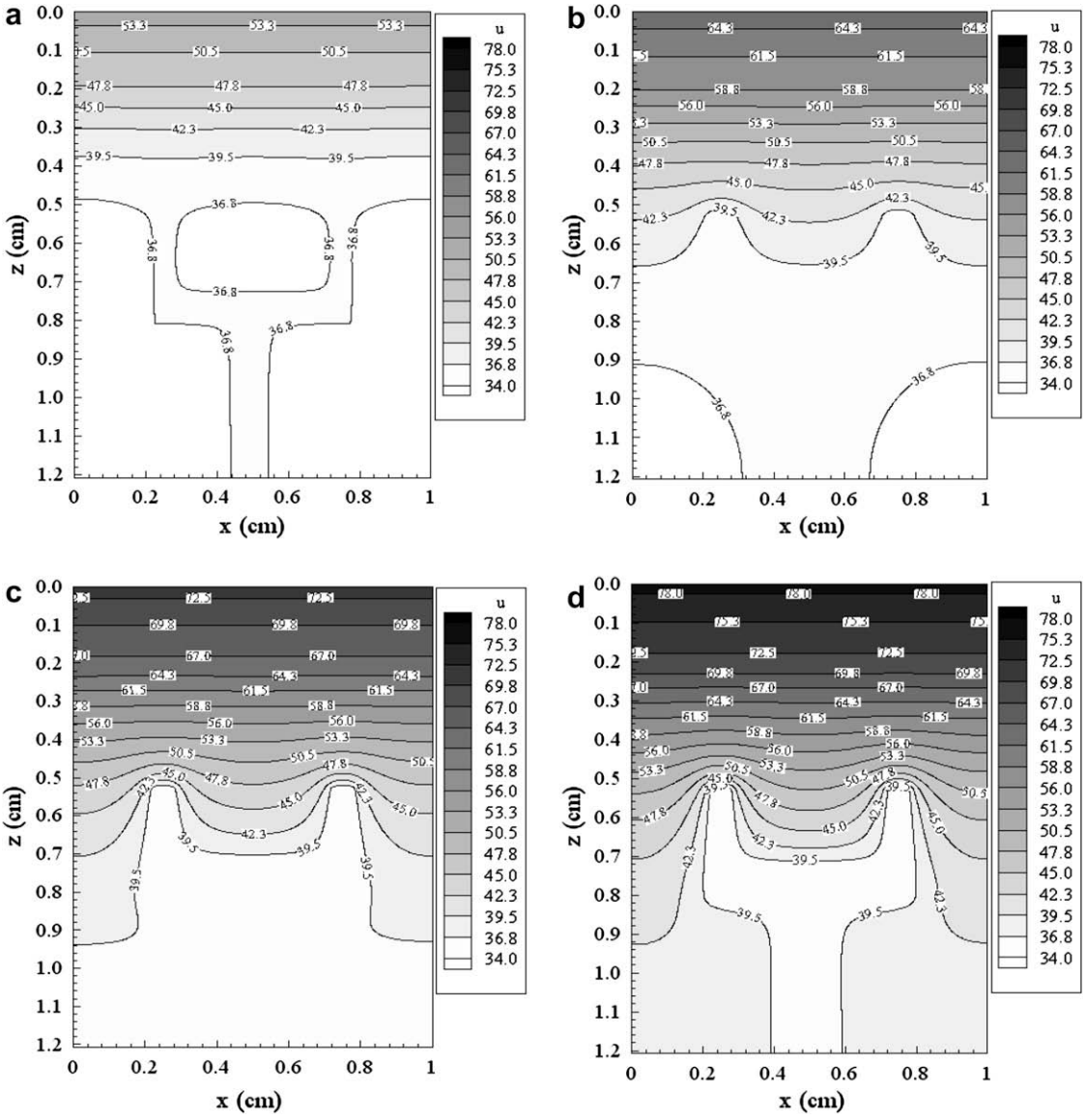

Fig. 5. Contours of the temperature distributions in the xz-cross-section at $y = 0.4$ cm, where the artery is located, at various times: (a) $t = 100$ s, (b) $t = 200$ s, (c) $t = 300$ s, and (d) $t = 400$ s.

$$\frac{(s_l)_{ijk}^{n+1}+(s_l)_{ijk}^{n}}{2} = \left(1+\tau\frac{W_b^l C_b^l}{\rho_l C_l}\right)\frac{(u_l)_{ijk}^{n+1}+(u_l)_{ijk}^{n}}{2}+\tau\frac{(u_l)_{ijk}^{n+1}-(u_l)_{ijk}^{n}}{\Delta t}, \tag{22}$$

$$\rho_l C_l\frac{(s_l)_{ijk}^{n+1}-(s_l)_{ijk}^{n}}{\Delta t}+W_b^l C_b^l\left[\frac{(u_l)_{ijk}^{n+1}+(u_l)_{ijk}^{n}}{2}-(u_b)_{out}\right] = k_l(\delta_x^2+\delta_y^2+\delta_z^2)\frac{(u_l)_{ijk}^{n+1}+(u_l)_{ijk}^{n}}{2}, \quad l=1,2,3, \tag{23}$$

where $(s_l)_{ijk}^{n}$ is the numerical approximation of $(S_l)(i\Delta x, j\Delta y, k\Delta z, n\Delta t)$, $\delta_x^2 u_{ijk}=\frac{1}{\Delta x^2}(u_{i+1jk}-2u_{ijk}+u_{i-1jk})$ and so on for the y and z directions. It should be pointed out that Eqs. (22) and (23) are unconditionally stable with a second-order truncation error. The proof can be referred to [41,42]. The discrete interfacial equations for Eqs. (17a) and (17b) are assumed to be, for any time level,

$$k_1\frac{(u_1)_{ijN_1^z}^{n}-(u_1)_{ijN_1^z-1}^{n}}{\Delta z}=k_2\frac{(u_2)_{ij1}^{n}-(u_2)_{ij0}^{n}}{\Delta z}, \quad (u_1)_{ijN_1^z}^{n}=(u_2)_{ij0}^{n}, \tag{24a}$$

and when the grid point (i,j) is in the tissue

$$k_2\frac{(u_2)_{ijN_2^z}^{n}-(u_2)_{ijN_2^z-1}^{n}}{\Delta z}=k_3\frac{(u_3)_{ij1}^{n}-(u_3)_{ij0}^{n}}{\Delta z}, \quad (u_2)_{ijN_2^z}^{n}=(u_3)_{ij0}^{n}. \tag{24b}$$

The interfacial condition, Eq. (16), between the tissue and the lateral blood vessel is discretized as follows:

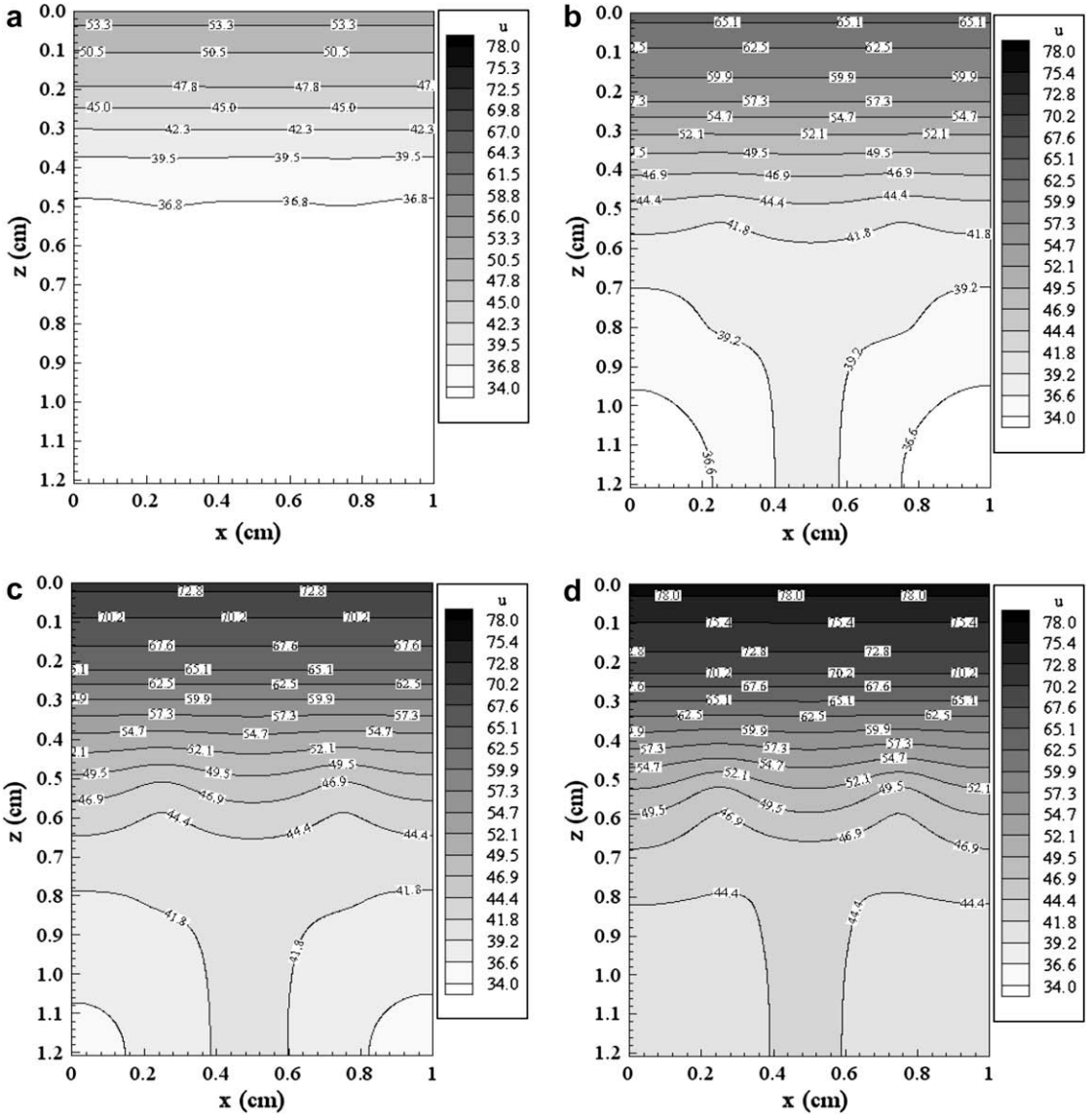

Fig. 6. Contours of the temperature distributions in the xz-cross-section at $y=0.5$ cm at various times: (a) $t=100$ s, (b) $t=200$ s, (c) $t=300$ s, and (d) $t=400$ s.

$$(u_3)_{ijk}^{n+1} = \left[(u_3)_{i+1jk}^{n+1} + Bi \cdot \Delta x \cdot (u_3)_{i-1jk}^{n+1}\right] \Big/ (1 + Bi \cdot \Delta x), \tag{25a}$$

$$(u_3)_{ijk}^{n+1} = \left[(u_3)_{ij+1k}^{n+1} + Bi \cdot \Delta y \cdot (u_3)_{ij-1k}^{n+1}\right] \Big/ (1 + Bi \cdot \Delta y), \tag{25b}$$

$$(u_3)_{ijk}^{n+1} = \left[(u_3)_{ijk+1}^{n+1} + Bi \cdot \Delta z \cdot (u_3)_{ijk-1}^{n+1}\right] \Big/ (1 + Bi \cdot \Delta z), \tag{25c}$$

where the grid point (i,j,k) is on the lateral walls of the blood vessel in the x, y, z directions, respectively. The top boundary condition is discretized as follows:

$$k_1 \frac{(u_1)_{ij1}^{n+1} - (u_1)_{ij0}^{n+1}}{\Delta z} = h\left[(u_1)_{ij0}^{n+1} - T_{\text{air}}\right] + \varepsilon\sigma\left\{T_{\text{a}}^2 + [(u_1)_{ij0}^{n}]^2\right\} \times \left[T_{\text{a}} + (u_1)_{ij0}^{n}\right]\left[T_{\text{a}} - (u_1)_{ij0}^{n+1}\right], \tag{26}$$

for any time level n.

Finally, Eq. (19) is discretized as follows:

$$\frac{\Omega_{ijk}^{n+1} - \Omega_{ijk}^{n}}{\Delta t} = \zeta \exp\left(-\frac{\Delta E}{R\frac{(T_l)_{ijk}^{n+1} + (T_l)_{ijk}^{n}}{2}}\right). \tag{27}$$

To decrease the computational time, we first solve for $(s_l)_{ijk}^{n+1}$ from Eq. (22), substitute it into Eq. (23)

$$\begin{aligned}\frac{\rho_l C_l}{\Delta t}\Bigg[&\left(1 + \tau\frac{W_{\text{b}}^l C_{\text{b}}^l}{\rho_l C_l} + \frac{2\tau}{\Delta t}\right)(u_l)_{ijk}^{n+1} \\ &+ \left(1 + \tau\frac{W_{\text{b}}^l C_{\text{b}}^l}{\rho_l C_l} - \frac{2\tau}{\Delta t}\right)(u_l)_{ijk}^{n} - 2(s_l)_{ijk}^{n}\Bigg] \\ &+ W_{\text{b}}^l C_{\text{b}}^l\left[\frac{(u_l)_{ijk}^{n+1} + (u_l)_{ijk}^{n}}{2} - (u_{\text{b}})_{\text{out}}\right] \\ &= k_l(\delta_x^2 + \delta_y^2 + \delta_z^2)\frac{(u_l)_{ijk}^{n+1} + (u_l)_{ijk}^{n}}{2}, \quad l = 1,2,3\end{aligned} \tag{28}$$

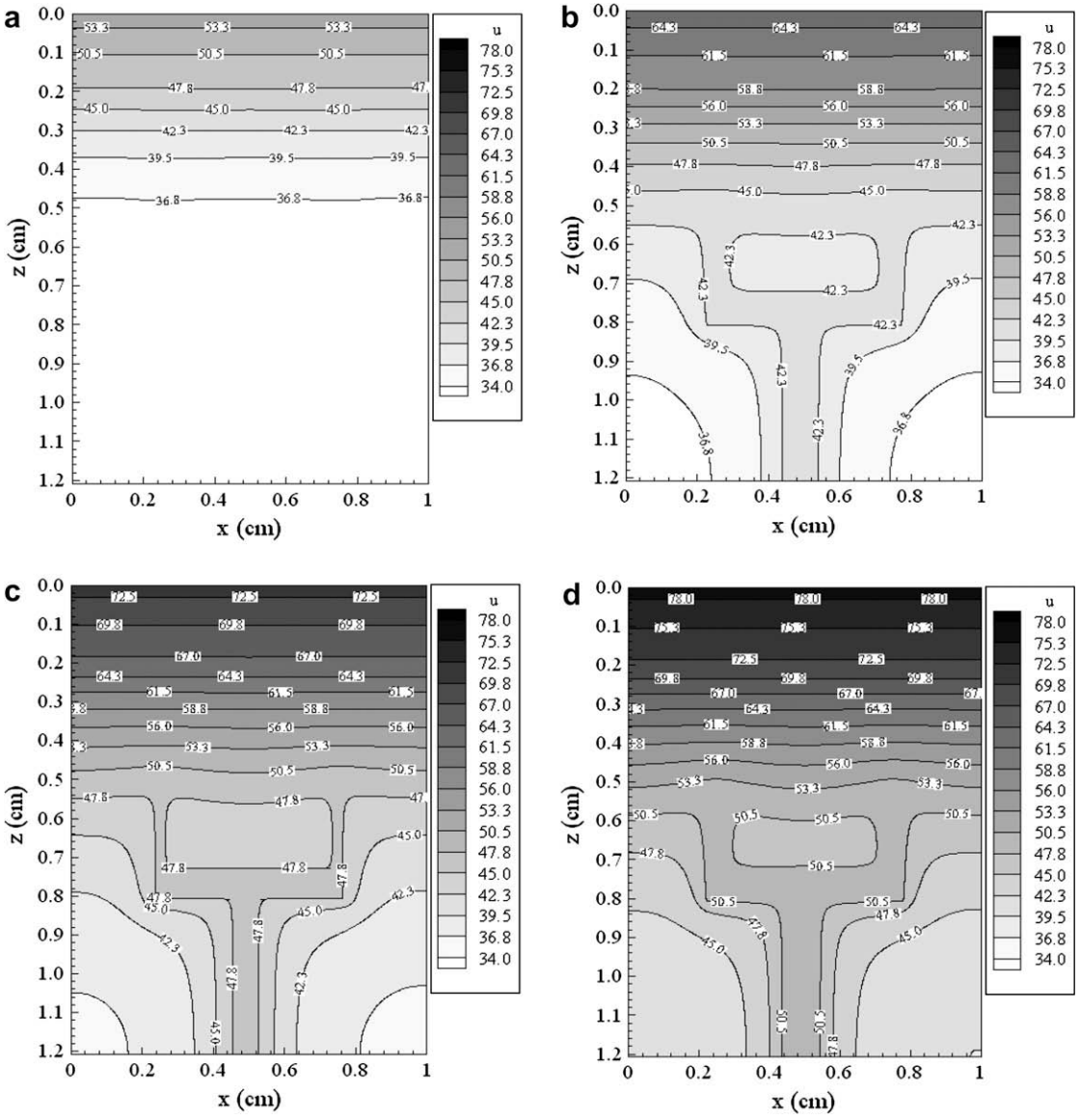

Fig. 7. Contours of the temperature distributions in the xz-cross-section at $y = 0.56$ cm, where the vein is located, at various times: (a) $t = 100$ s, (b) $t = 200$ s, (c) $t = 300$ s, and (d) $t = 400$ s.

and then employ a preconditioned Richardson iteration described in [43–45] as follows:

$$
\begin{aligned}
&L^1_{\mathrm{pre}}\left[(u_l)^{n+1}_{ijk}\right]^{(I+1)} \\
&\quad = L^1_{\mathrm{pre}}\left[(u_l)^{n+1}_{ijk}\right]^{(I)} - \omega\left\{\frac{\rho_l C_l}{\Delta t}\left[\left(1+\tau\frac{W^l_{\mathrm{b}}C^l_{\mathrm{b}}}{\rho_l C_l}+\frac{2\tau}{\Delta t}\right)[(u_l)^{n+1}_{ijk}]^{(I)}\right.\right. \\
&\qquad +\left(1+\tau\frac{W^l_{\mathrm{b}}C^l_{\mathrm{b}}}{\rho_l C_l}-\frac{2\tau}{\Delta t}\right)(u_l)^n_{ijk} - 2(s_l)^n_{ijk}\Big] \\
&\qquad + W^l_{\mathrm{b}}C^l_{\mathrm{b}}\left[\frac{[(u_l)^{n+1}_{ijk}]^{(I)}+(u_l)^n_{ijk}}{2} - (u_{\mathrm{b}})_{\mathrm{out}}\right] \\
&\qquad \left.-k_l(\delta^2_x+\delta^2_y+\delta^2_z)\frac{[(u_l)^{n+1}_{ijk}]^{(I)}+(u_l)^n_{ijk}}{2}\right\},
\end{aligned}
\tag{29}
$$

where ω is the relaxation factor, and the preconditioner is chosen to be

$$
\begin{aligned}
L^1_{\mathrm{pre}} &= 1+\tau\frac{W^l_{\mathrm{b}}C^l_{\mathrm{b}}}{\rho_l C_l}+\frac{2\tau}{\Delta t}+\frac{W^l_{\mathrm{b}}C^l_{\mathrm{b}}\Delta t}{2\rho_l C_l} \\
&\quad +\frac{2k_l\Delta t}{\rho_l C_l}\left(\frac{1}{\Delta x^2}+\frac{1}{\Delta y^2}\right)-\frac{k_l\Delta t}{2\rho_l C_l}\delta^2_z.
\end{aligned}
\tag{30}
$$

As such, the linear system, Eq. (28), can be transferred into many tridiagonal linear systems. Noted that we denote $(u_3)^n_{ijk}=(u^m_{\mathrm{b}})_{ijk}$ when the grid point (i,j,k) is in the mth level blood vessel, the Thomas algorithm can be used line by line along the z-direction. Our algorithm for predicting the skin burning in a 3D skin structure induced by radiation heating can be described as follows:

Step 1. Assume the wall temperature of the blood vessel u^m_{w}. Obtain the blood temperature u^m_{b}, by solving Eqs. (9)–(11) using the fourth-order Runge–Kutta method. Then obtain the temperature

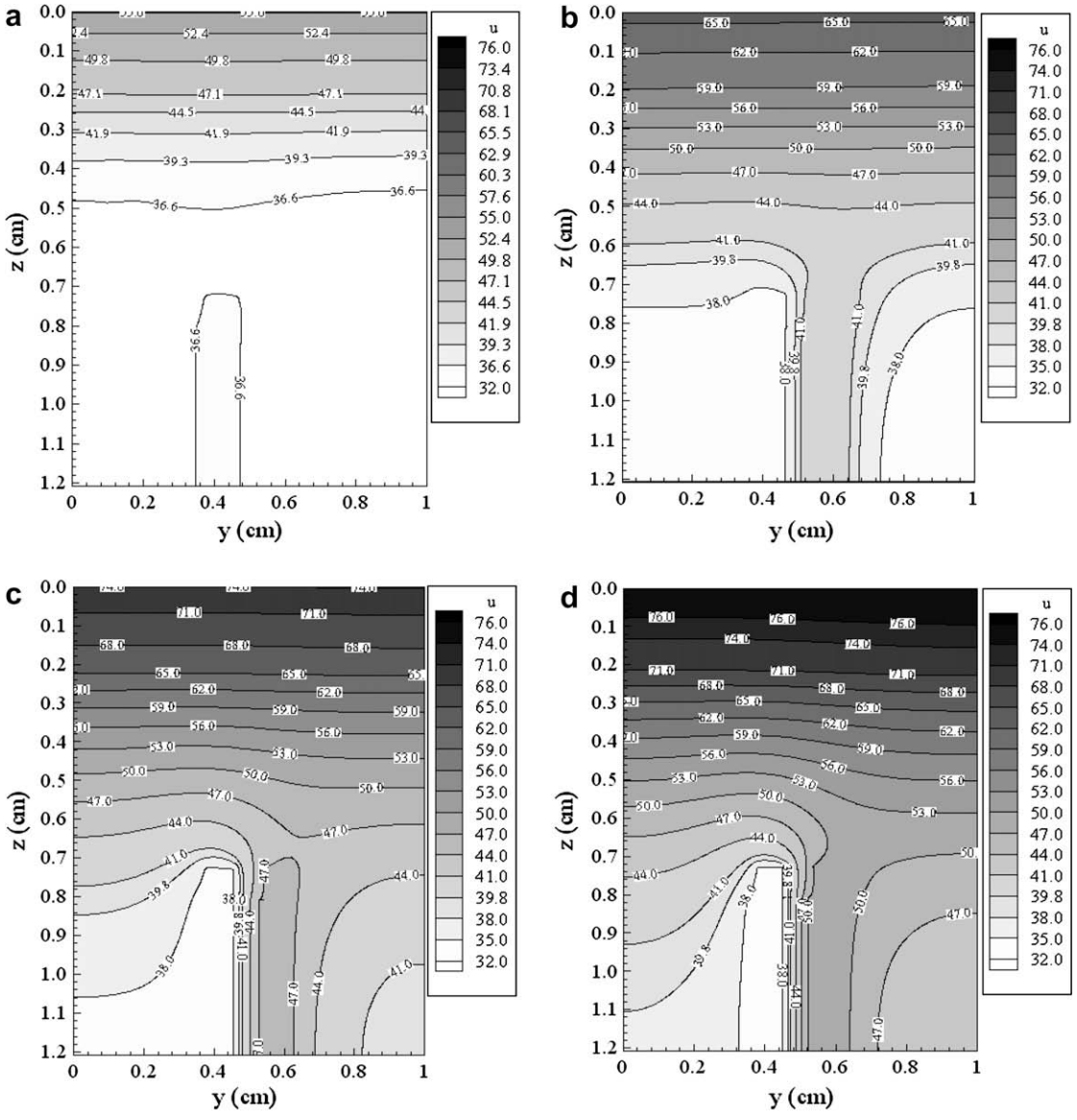

Fig. 8. Contours of the temperature distributions in the yz-cross-section at $x=0.5$ cm at various times: (a) $t=100$ s, (b) $t=200$ s, (c) $t=300$ s, and (d) $t=400$ s.

distribution $\vec{u}$ in the entire 3D skin structure by solving Eqs. (22) and (29) coupled with the interfacial equations, Eqs. (24a) and (24b), and the initial and boundary conditions.

Step 2. Update the wall temperature of the blood vessel, u_w^m, by Eqs. (25a)–(25c).

Step 3. Repeat steps 1 and 2 until a convergent solution, $\vec{u}$, at time level $n+1$ is obtained.

Step 4. Calculate the damage function Ω by Eq. (27).

4. Numerical example

To test our algorithm, we chose a 3D composite skin structure, as shown in Fig. 2, with the dimensions 1 cm × 1 cm × 1.208 cm. The values of the biological parameters used are given in Table 1. In our computation, we considered heat transfer by convection from the skin's surface ($h = 0.001$ W/cm^2 [33]), where the surface is exposed to an ambient temperature of 200 °C, along with radiation heating. Additionally, the thermal relaxation time and emissivity were taken to be $\tau = 20$ s [21] and $\varepsilon = 0.9$ [39], respectively. Three meshes of 50 × 50 × 1208, 50 × 100 × 1208, and 100 × 100 × 1208 were chosen in order to test the convergence of the solution. Other parameters used in our computation are listed in Tables 2 and 3.

Fig. 3 shows the temperature profiles at $t = 200$ s along the lines (a) $y = 0.5$ cm and (b) $x = 0.5$ cm on the skin surface, and (c) along the depth (the z-direction) at the center of the skin surface, respectively, as well as (d) the temperature profiles over time at the point, where $x = 0.5$ cm, $y = 0.5$ cm, and $z = 0.1$ cm. It can be seen from this figure

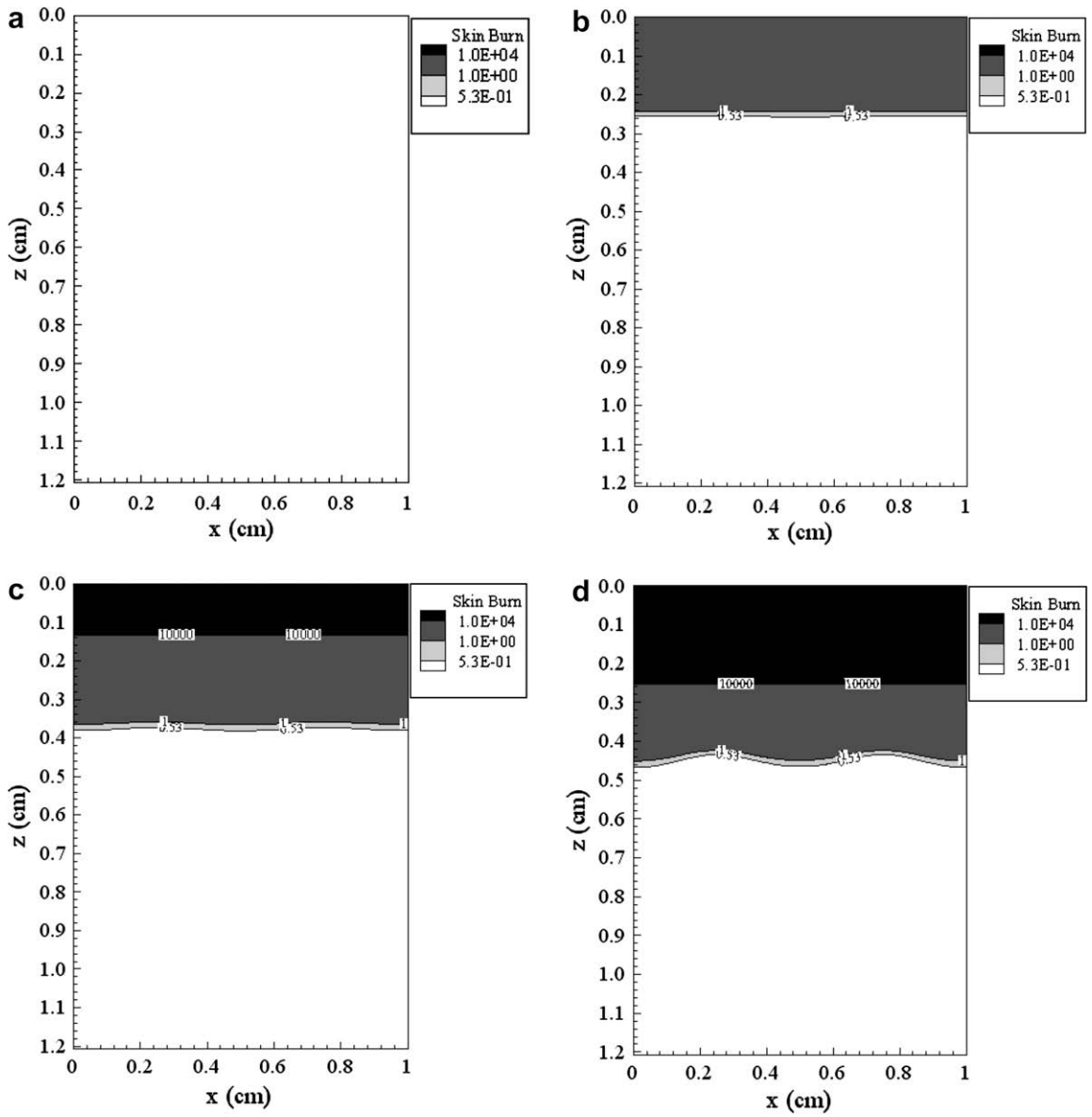

Fig. 9. Contours of the skin burn distributions in the xz-cross-section at $y = 0.4$ cm, where the artery is located, at various times: (a) $t = 100$ s, (b) $t = 200$ s, (c) $t = 300$ s, and (d) $t = 400$ s.

that there are no significant differences in the solutions obtained based on these three meshes, implying the solution is independent of the mesh size.

Fig. 4 shows the comparison of the solutions verses time at (a) $x = 0.5$ cm, $y = 0.5$ cm, and $z = 0$ cm, and (b) $x = 0.5$ cm, $y = 0.5$ cm, and $z = 0.1$ cm, where the solutions were obtained based on the Pennes equation, Eq. (4), and the modified Pennes equation, Eq. (5), respectively. Comparing these two solutions, we see that there is a time delay in the solution obtained by the modified Pennes equation.

Fig. 5 shows the contours of the temperature distributions in these xz -cross-sections at $y = 0.40$ cm, where the artery is located, at various times (a) $t = 100$ s, (b) $t = 200$ s, (c) $t = 300$ s, and (d) $t = 400$ s. Fig. 6 shows the contours of the temperature distributions in the xz-cross-section at $y = 0.5$ cm at various times (a) $t = 100$ s, (b) $t = 200$ s, (c) $t = 300$ s, and (d) $t = 400$ s. Fig. 7 shows the contours of the temperature distributions at $y = 0.56$ cm, where the vein is located, at various times (a) $t = 100$ s, (b) $t = 200$ s, (c) $t = 300$ s, and (d) $t = 400$ s. Fig. 8 shows the contours of the temperature distributions at the yz-cross-section at $x = 0.5$ cm, at various times (a) $t = 100$ s, (b) $t = 200$ s, (c) $t = 300$ s, and (d) $t = 400$ s. It can be seen from these figures that the temperature profiles are symmetric in the xz-cross-section at $y = 0.5$ cm, and the temperature elevations around the region where the vein is located are higher than those around the region where the artery is located. This implies that the vein is carrying the heat out, away from the heated area, and into the body core.

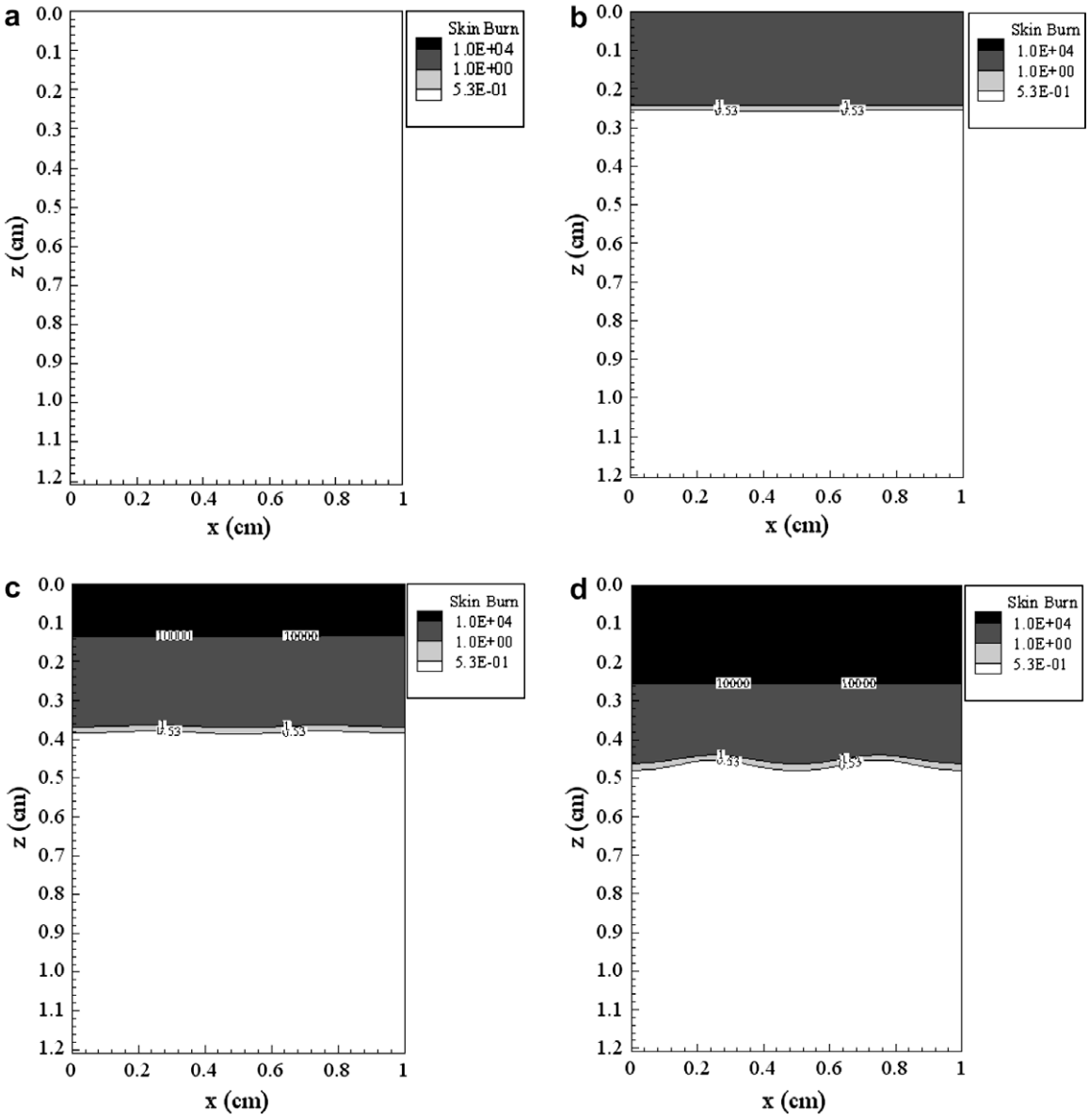

Fig. 10. Contours of the skin burn distributions in the xz-cross-section at $y = 0.5$ cm at various times: (a) $t = 100$ s, (b) $t = 200$ s, (c) $t = 300$ s, and (d) $t = 400$ s.

Figs. 9–12 show the contours of the damage corresponding to Figs. 5–8 showing the temperature distributions. Since values of $\Omega = 0.53$, 1.0, 10^4 correspond to the first, second, and third degree burn injuries, respectively [39], one may see from these figures that the skin appears to be second burn at $t = 200$ s, and the third degree burn at $t = 300$ s and $t = 400$ s.

5. Conclusion

In this study, we have developed a mathematical model for predicting the temperature of, and thermal damage suffered by, skin due to radiation heating. The model takes into account the relatively large thermal relaxation time of biological tissue and the effects of high thermal radiation on such tissue using the Maxwell–Cattaneo thermal flux law in conjunction with the fourth power law. The tissue is considered to be a 3D, triple-layered skin structure wherein are embedded countercurrent multi-level blood vessels, arteries and veins. Further, the dimensions and blood flow rates were determined based on the constructal theory of multi-scale tree-shaped heat exchangers.

Our numerical results show that the classic Pennes equation predicts a greater temperature than the modified (i.e., Maxwell–Cattaneo based) equation (see Fig. 4). Additionally, the latter equation exhibits the expected time delay in the temperature solution (see Fig. 4b).

The exploratory approach developed in this paper could be used in future studies: e.g., by considering a larger area of skin structure, with more complicated dendritic countercurrent multi-level blood vessels, as well as modeling such

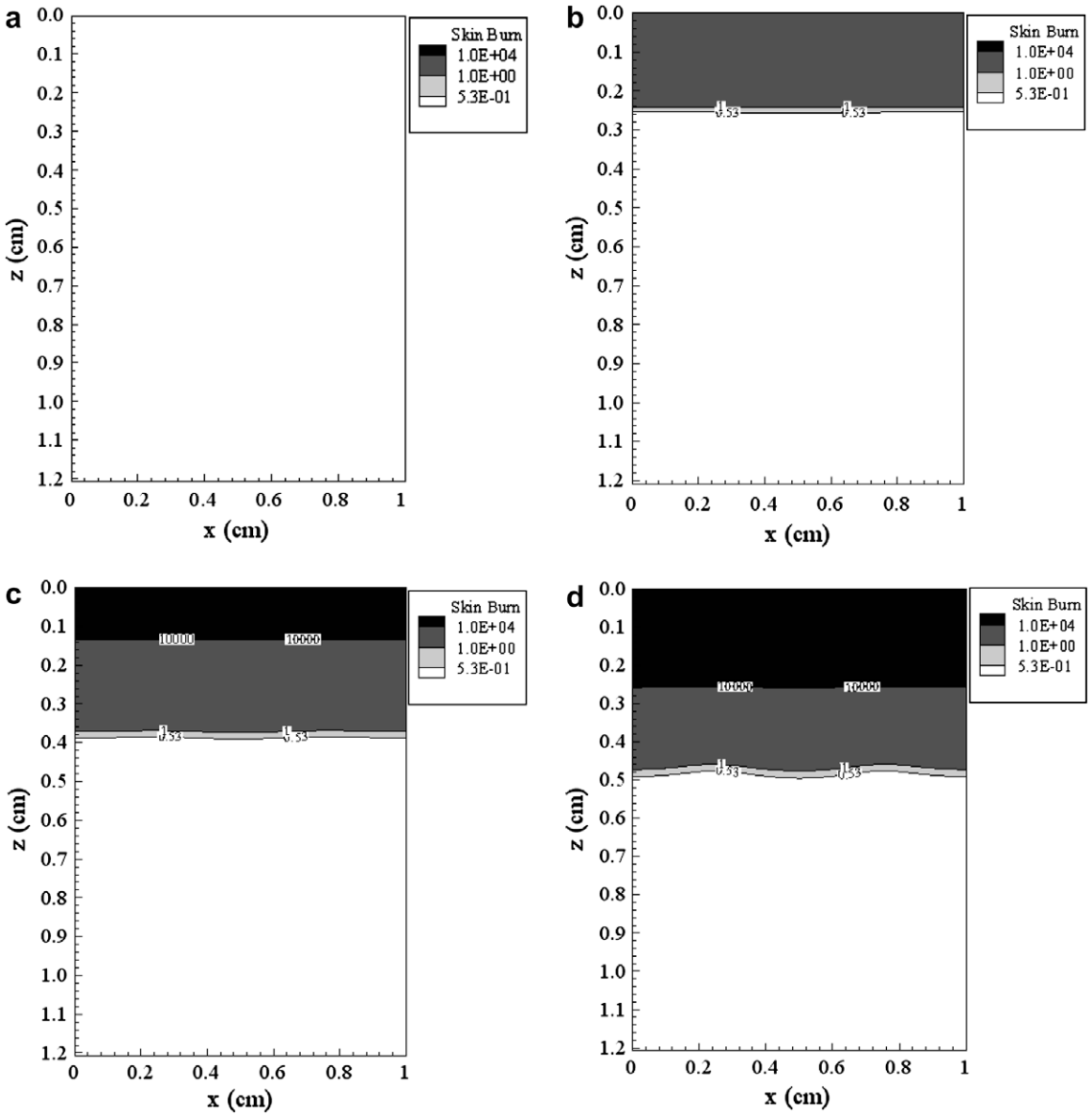

Fig. 11. Contours of the skin burn distributions in the xz-cross-section at $y = 0.56$ cm, where the vein is located, at various times: (a) $t = 100$ s, (b) $t = 200$ s, (c) $t = 300$ s, and (d) $t = 400$ s.

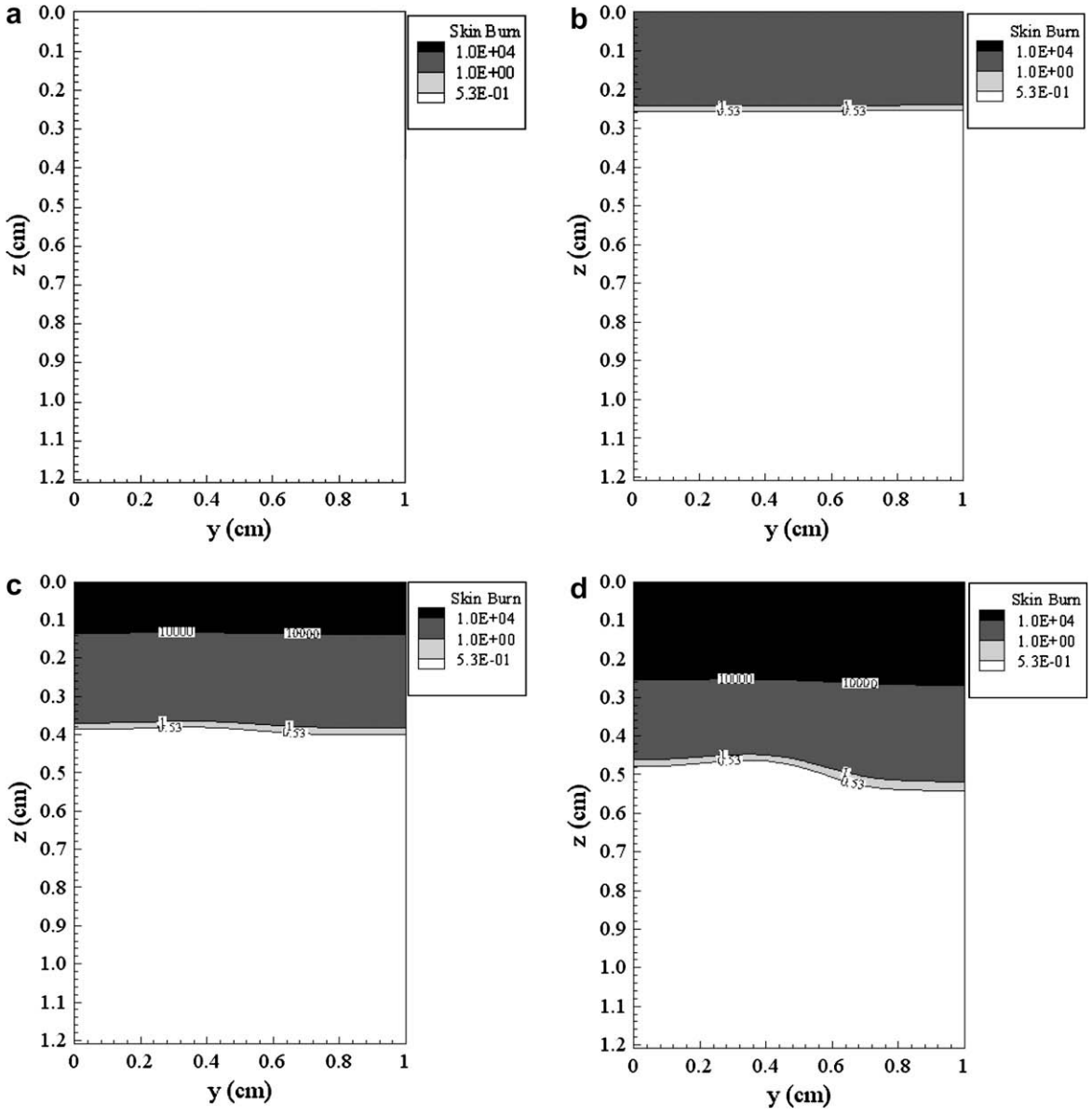

Fig. 12. Contours of the skin burn distributions in the yz-cross-section at $x = 0.5$ cm at various times: (a) $t = 100$ s, (b) $t = 200$ s, (c) $t = 300$ s, and (d) $t = 400$ s.

well documented effects of thermal damage as skin wrinkles and tissue shrinkage.

References

[1] R.C. Borkebak, Heat transfer in biological systems, Int. Rev. Gen. Exper. Zool. 2 (1966) 269–344.
[2] H.F. Bowman, E.G. Cravalho, M. Woods, Theory, measurement and application of properties of biomaterials, Ann. Rev. Biophys. Bioeng. 4 (1975) 43–80.
[3] K. Mitra et al., Experimental evidence of hyperbolic heat conduction in processed meat, Trans. ASME J. Heat Transfer 117 (1995) 568–573.
[4] P.J. Antaki, Hotter than you think, Mach Des 13 (July) (1995) 116–118.
[5] C. Cattaneo, Sullaconduzione de calore, Atti del Seminar, vol. 3, Mat. Fis. University, Modena, 1948, pp. 83–101.
[6] P. Vernotte, Les paradoxes de la theorie continue de L'equation de la chaleur, Compute Rendus 246 (1958) 3145–3155.
[7] D.S. Chandrasekharaiah, Thermoelasticity with second sound: a review, Appl. Mech. Rev. 39 (1986) 355–376.
[8] D.S. Chandrasekharaiah, Hyperbolic thermoelasticity: a review of recent literature, Appl. Mech. Rev. 51 (1998) 705–729.
[9] D.D. Joseph, L. Preziosi, Heat waves, Rev. Mod. Phys. 61 (1989) 41–73.
[10] D.D. Joseph, L. Preziosi, Addendum to the paper "heat waves", Rev. Mod. Phys. 62 (1990) 375–391.
[11] W. Dreyer, H. Struchtrup, Heat pulse experiments revisited, Cont. Mech. Thermodyn. 5 (1993) 3–50.
[12] D.Y. Tzou, Macro- to Microscale Heat Transfer: The Lagging Behavior, Taylor & Francis, Washington, DC, 1996.
[13] C.I. Christov, P.M. Jordan, Heat conduction paradox involving second-sound propagation in moving media, Phys. Rev. Lett. 94 (2005) 54301.
[14] H.H. Pennes, Analysis of tissue and arterial temperature in the resting human forearm, J. Appl. Physiol. 1 (1948) 93–122.
[15] W. Wulff, The energy conservation equation for living tissues, IEEE Trans. Biomed. Eng. 21 (1974) 494–495.

[16] S. Weinbaum, L.M. Jiji, A new simplified bioheat equation for the effect of blood flow on a local average tissue temperature, J. Biomed. Eng. 107 (1985) 131–139.
[17] J.W. Baish, P.S. Ayyaswamy, K.R. Foster, Heat transfer mechanisms in vascular tissues: a model comparison, J. Biomed. Eng. 108 (1986) 246–250.
[18] J.W. Baish, P.S. Ayyaswamy, K.R. Foster, Small-scale temperature fluctuations in perfused tissue during local hyperthermia, J. Biomed. Eng. 108 (1986) 324–331.
[19] M.M. Chen, K.R. Holmes, Microvascular contributions in tissue heat transfer, Ann. NY Acad. Sci. 335 (1980) 137–150.
[20] C.K. Charny, Mathematical models of bioheat transfer, in: Y. I Cho, J.P. Hartnett, T.F. IrvineJr. (Eds.), Advanced in Heat Transfer, vol. 22, Academic Press, New York, 1992, pp. 19–155.
[21] J. Liu, X. Chen, L.X. Xu, New thermal wave aspects on burn evaluation of skin subjected to instantaneous heating, IEEE Trans. Biomed. Eng. 46 (1999) 420–428.
[22] J. Liu, Preliminary survey on the mechanisms of the wave-like behaviors of heat transfer in living tissues, Forsch. Ingenieurwesen 66 (2000) 1–10.
[23] Z. Deng, J. Liu, Numerical simulation of 3-D freezing and heating problems for combined cryosurgery and hyperthermia therapy, Numer. Heat Transfer, Part A 46 (2004) 587–611.
[24] S. Karaa, J. Zhang, F. Yang, A numerical study of a 3D bioheat transfer problem with different spatial heating, Math. Comput. Simul. 68 (2005) 375–388.
[25] W. Shen, J. Zhang, F. Yang, Modeling and numerical simulation of bioheat transfer and biomechanics in soft tissue, Math. Comput. Model. 41 (2005) 1251–1265.
[26] A. Bejan, Shape and Structure from Engineering to Nature, Cambridge University Press, Cambridge, UK, 2000.
[27] A. Bejan, The tree of convective heat streams: its thermal insulation function and the predicted $\frac{3}{4}$-power relation between body heat loss and body size, Int. J. Heat Mass Transfer 44 (2001) 699–704.
[28] A.K. da Silva, S. Lorente, A. Bejan, Constructal multi-scale tree-shaped heat exchangers, J. Appl. Phys. 96 (2004) 1709–1718.
[29] A. Bejan, S. Lorente, Constructal theory of generation of configuration in nature and engineering, J. Appl. Phys. 100 (2006) 041301.
[30] L.P. Gartner, Color Atlas of Histology, 3rd ed., Lippincott Williams & Wilkins, Philadelphia, 2000.
[31] L.T. Lorimer, The Human Body, Reader's Digest, New York, 1999.
[32] J. Zhou, J. Liu, Numerical study on 3-D light and heat transport in biological tissues with large blood vessels during laser-induced thermotherapy, Numer. Heat Transfer, Part A 45 (2004) 415–449.
[33] H.W. Huang, Z.P. Chen, R.B. Roemer, A counter current vascular network model of heat transfer in tissues, J. Biomech. Eng. 118 (1996) 120–129.
[34] H.W. Huang, Convective thermal model formulation of a three dimensional vascular system with simplified blood flow paths: temperature distributions during hyperthermia, MS Thesis, University of Arizona, Tucson, AZ, 1992.
[35] E. Majchrzak, B. Mochnacki, Numerical model of heat transfer between blood vessel and biological tissue, Comput. Assist. Mech. Eng. Sci. 6 (1999) 439–447.
[36] C. Sturesson, A. Andersson-Engels, A mathematical model for predicting the temperature distribution in laser-induced hyperthermia: experimental evaluation and applications, Phys. Med. Biol. 40 (1995) 2037–2052.
[37] H.W. Huang, C.L. Chan, R.B. Roemer, Analytical solutions of Pennes bioheat transfer equation with a blood vessel, J. Biomech. Eng. 116 (1994) 208–212.
[38] F.C. Henriques, A.R. Mortiz, Studies of thermal injury in the conduction of heat to and through skin and the temperature attained therein: a theoretical and experimental investigation, Amer. J. Pathol. 23 (1947) 531–549.
[39] K.R. Diller, Modeling of bioheat transfer processes at high and low temperature, in: Y. I Cho, J.P. Hartnett, T.F. IrvineJr. (Eds.), Advanced in Heat Transfer, vol. 22, Academic Press, New York, 1992, pp. 157–357.
[40] R.L. Burden, D.J. Faires, Numerical Analysis, seventh ed., Brooks/Cole, 2001 (Chapter 5).
[41] W. Dai, R. Nassar, A finite difference scheme for solving the heat transport equation at the microscale, Numer. Meth. Partial Diff. Eq. 15 (1999) 597–708.
[42] W. Dai, R. Nassar, An unconditionally stable finite difference scheme for solving a 3D heat transport equation in a sub-microscale thin film, J. Comp. Appl. Math. 145 (2002) 247–260.
[43] L. Zhang, W. Dai, R. Nassar, A numerical modeling for optimizing laser power irradiating on a 3D triple layered cylindrical skin structure, Numer. Heat Transfer, Part A 48 (2005) 21–41.
[44] L. Zhang, W. Dai, R. Nassar, A numerical method for obtaining an optimal temperature distribution in a 3D triple layered cylindrical skin structure embedded with a blood vessel, Numer. Heat Transfer, Part A 49 (2006) 437–465.
[45] W. Dai, A. Bejan, X. Tang, L. Zhang, R. Nassar, Optimal temperature distribution in a 3D triple layered skin structure with embedded vasculature, J. Appl. Phys. 99 (2006) 104702.
[46] X. Tang, W. Dai, R. Nassar, A. Bejan, Optimal temperature distribution in a 3D triple layered skin structure embedded with artery and vein vasculature, Numer. Heat Transfer, Part A 50 (2006) 809–843.